JOURNAL OF PROPULSION AND POWER
Vol. 26, No. 6, November–December 2010

Experimental Study of Cavity-Strut Combustion in Supersonic Flow

K. -Y. Hsu*
Innovative Scientific Solutions, Inc., Dayton, Ohio 45440
and
C. D. Carter,† M. R. Gruber,† T. Barhorst,‡ and S. Smith‡
U.S. Air Force Research Laboratory, Wright-Patterson Air Force Base, Ohio 45433

DOI: 10.2514/1.45767

An experimental investigation of cavity-based flameholders with strut injectors in a supersonic flow is reported. In this ongoing research program, emphasis is placed on understanding cavity-based flameholders and providing alternative methods for improving overall combustor performance in scramjet engines. Three different struts with fuel injectors are mounted near the cavity leading edge to study flame propagation and ignition of fuel in the core flow region. Planar laser-induced fluorescence of the OH radical is used to identify the flame zone around the cavity and strut-wake regions over a range of conditions. Shadowgraphy is employed to capture the flow features around the strut and cavity. In-stream probing is conducted to characterize the flow features associated with the different strut configurations. Stagnation-temperature profiles are obtained for all struts operating under the same condition in the combusting-flow study. Two cavity fueling schemes are used to compare flameholder performance. Direct cavity air injection is found to improve combustion significantly. For each strut, upstream and downstream fueling schemes are compared over a range of conditions. Overall, successful combustion is observed in the strut-wake region using upstream strut-fueling schemes for the three struts employed in this study.

I. Introduction

CAVITY-BASED flameholders are commonly used in hydrocarbon-fueled scramjet combustors; however, detailed information concerning the behavior of these devices, their optimal shape and fueling strategies, combustion stability, interactions with disturbances in the main air flow (i.e., shock trains or shock-boundary layer interactions), and capability of ignition and sustained main combustion is largely unavailable in the existing literature. Studies [1–4] of cavity-based flameholders in supersonic flows conducted at the U.S. Air Force Research Laboratory (AFRL) have shown that the combustion around a flameholder can be optimized through the use of the proper fueling method.

Development of a flameholder that exhibits stable operation over a broad range of conditions and that is capable of effective ignition and sustained main combustion at lower Mach numbers requires study of the coupling mechanism between the flameholder and the main air/fuel streams. The shear layer that is formed at the interface between the cavity and core flow has been identified as a critical region in the development of efficient flameholder in scramjet engines. This shear-layer plays an important role in transferring mass and energy into and out of the cavity. The air entrained into the cavity results from the interaction between the shear layer and the cavity, which directly affects the mixing and stoichiometry inside the cavity. The exchange of species and energy between the core flow and the cavity can have a direct impact on the operating limit of the flameholder and ignition of the scramjet combustor.

Fuel injection in the scramjet combustor has been studied for decades, with the main emphasis having been placed on mixing and efficient combustion. To achieve fueling in the supersonic core region, strut injectors have been used to improve fuel distribution and mixing [5–8].

The main objective of the present study was to examine the coupling between the cavity and the strut-injected fuel as well as the potential for improving combustion in a scramjet engine. Conventional and advanced diagnostics were used to characterize the interactions between the cavity and the wake region created by struts.

II. Experimental Description

An experimental study of a cavity-based flameholder was conducted in a supersonic research facility [1]. Continuous Mach 2 air flow was achieved via an asymmetrical two-dimensional facility nozzle that is connected upstream of the test section. Cavity-flameholder tests were conducted in a rectangular test section with optical windows located in three walls. The bottom wall consists of modular hardware that allows various test configurations to be installed and tested. The test section has a 17.78-cm-long constant-area section (5.08 cm high by 15.24 cm wide), followed by a 2.5-deg divergence on the bottom wall. The cavity flameholder and strut injector are located on the bottom wall (see Fig. 1).

Three different strut injectors were installed upstream of a baseline cavity, as illustrated in Fig. 1. The cavity extends 15.24 cm in the spanwise direction z, with a 90-deg leading edge and a 22.5-deg ramp at the trailing edge. The cavity is 1.65 cm. deep, and the length of the cavity floor is 4.57 cm. Three rows of injection ports are located along the cavity ramp for fuel and air injections. The middle row has 10 injectors, and the top and bottom rows have 11 injectors each. A separate manifold is used to supply each row independently. The 0.16-cm-diameter injection ports are parallel to the cavity floor. Spark plugs installed on the cavity floor are used for ignition.

The three struts have a 35-deg sweep angle and a 13.6-deg compression angle at the leading edge. The struts were installed flush with the floor upstream of the cavity, with the leading edge located 7.2 cm upstream of the cavity leading edge, as shown in Fig. 1. The struts are 2.4 cm high (from the tunnel floor) and 0.95 cm wide at the base. The main difference among the struts is the length and shape of the aft body. Strut 1 has a vertical trailing edge that is aligned with the

Presented as Paper 2007-5394 at the 43rd AIAA/ASME/SAE/ASEE Joint Propulsion Conference & Exhibit, Cincinnati, OH, 8–11 July 2007; received 1 June 2009; revision received 1 July 2010; accepted for publication 1 July 2010.

*Senior Research Scientist, 2766 Indian Ripple Road. Associate Fellow AIAA.
†Senior Aerospace Engineer, AFRL/RZAS, 1950 Fifth Street. Associate Fellow AIAA.
‡Engineer, AFRL/RZAS, 1950 Fifth Street. Member AIAA.

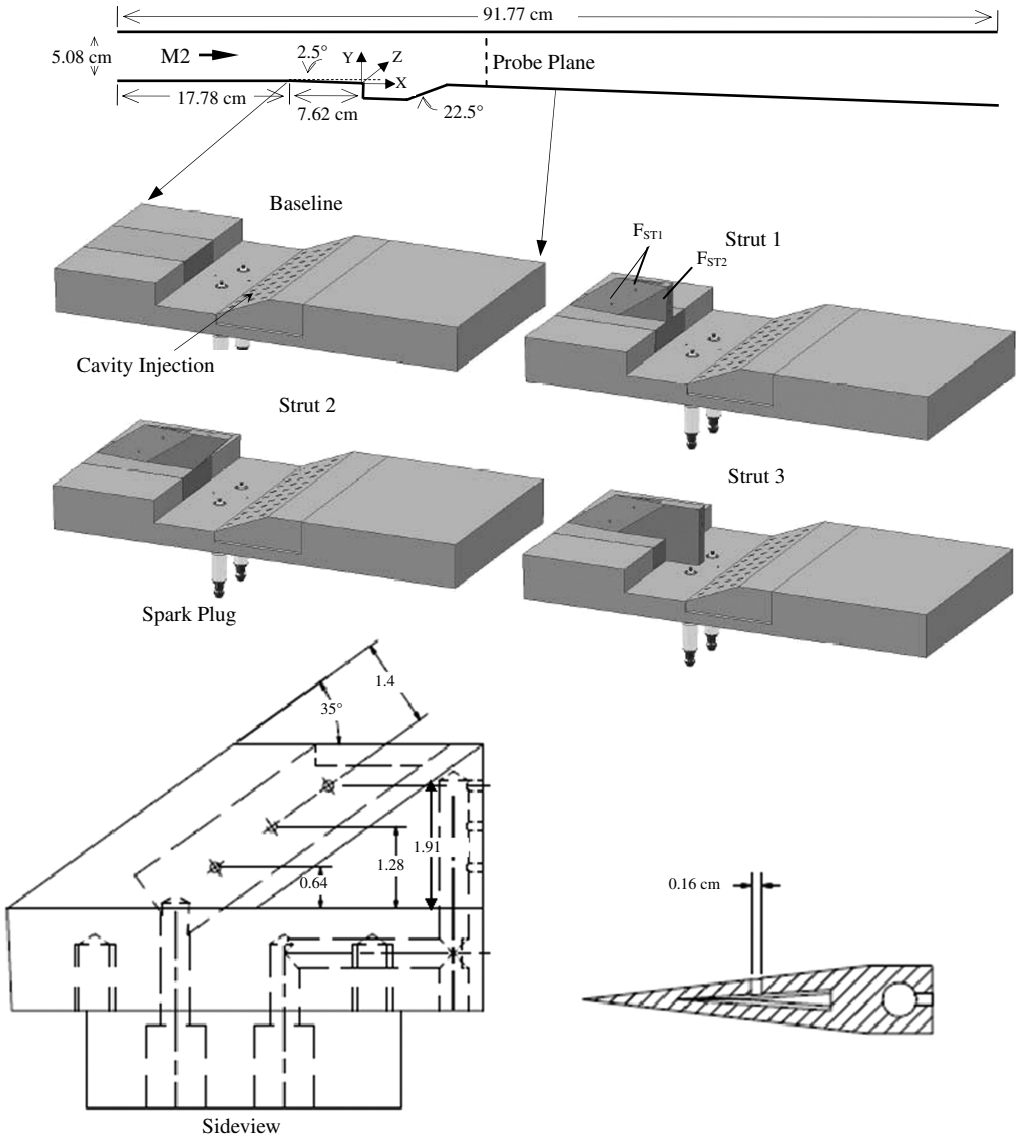

Fig. 1 Configurations of cavity and strut injectors.

cavity leading edge. Strut 2 has a 45-deg slanted trailing edge that extends over the top of the cavity. Strut 3 is similar to strut 1, except that it is 2.54 cm longer and extends to the floor of the cavity. Two fuel-injection schemes are employed for each strut. Three upstream fuel injectors F_{ST1} are located on the compression surface, with two on one side and one on the other, with a vertical spacing of 0.64 cm. Three downstream fuel injectors F_{ST2} are located at the base of the strut, with a vertical spacing of 0.64 cm. All injection ports are 0.16 cm in diameter, and the strut fuel is fed from two independent internal manifolds (one for ST1 and one for ST2).

Combustion tests were conducted at a nominal Mach 2 (design Mach number) inflow condition, with stagnation conditions of $P_0 = 483 \pm 4$ kPa and $T_0 = 590 \pm 1.5$ K. Velocities in this flowpath, under nonreacting conditions, are reported by Lahr et al. [9] and by Grady et al. [10]. Separate control/metering of fuel (ethylene) and air was used for cavity and strut-fuel injections. A mass flow controller was used to control and meter the cavity air injection. Critical venturi nozzles were employed to meter the ethylene flowrate, and the measured mass flow uncertainty was $\pm 1.4\%$ of the reading calculated, based on the procedure developed by AFRL/RZAS [11].

Planar laser-induced fluorescence (PLIF) was used to identify the OH distribution around the cavity and strut-wake regions over a range of injection conditions. For OH excitation, a Spectra-Physics GCR 170 laser pumped a Lumonics HD300 dye laser; the dye laser was tuned to 567 nm so that the frequency-doubled radiation matched the wavelength for the $Q_1(8)$ transition of the $A^2\Sigma^+ - X^2\Pi$ ($v' = 1$, $v'' = 0$) band. To ensure good overlap of the laser and transition, a portion of the UV beam was split off and directed over a small McKenna burner (reference flame) and then to a fast photodiode. Fluorescence from the reference flame was sampled with a photomultiplier tube; this signal, along with the photodiode output, was continuously displayed on an oscilloscope, allowing minor adjustments to be made to the dye laser grating position for mitigating the effects of temperature changes in the test environment. The laser probe sheet was formed with a simple two-lens telescope configuration (negative cylindrical lens followed by a positive 1-m spherical focusing lens). The laser sheet was then directed through the side-wall window for spanwise sheet measurements or through the top-wall window for streamwise sheet measurements. In both cases the fluorescence was viewed through the side window using a Princeton Instruments PIMAX intensified charge-coupled device (CCD) camera equipped with a Cerco 45-mm f/1.8 UV lens; Schott UG5 and WG305 filters were used to block visible radiation and background laser scattering. In the case of the spanwise measurements, the camera and lens were mounted on a Scheimpflug adaptor to mitigate blur concomitant with non-normal sheet viewing; here, the camera imaged fluorescence from a downstream viewing perspective at as shallow an angle (with the streamwise axis) as practical. The camera array, normally 512×512 pixels, was binned 2×2 to achieve a framing rate of 10 fps and match the laser pulse repetition

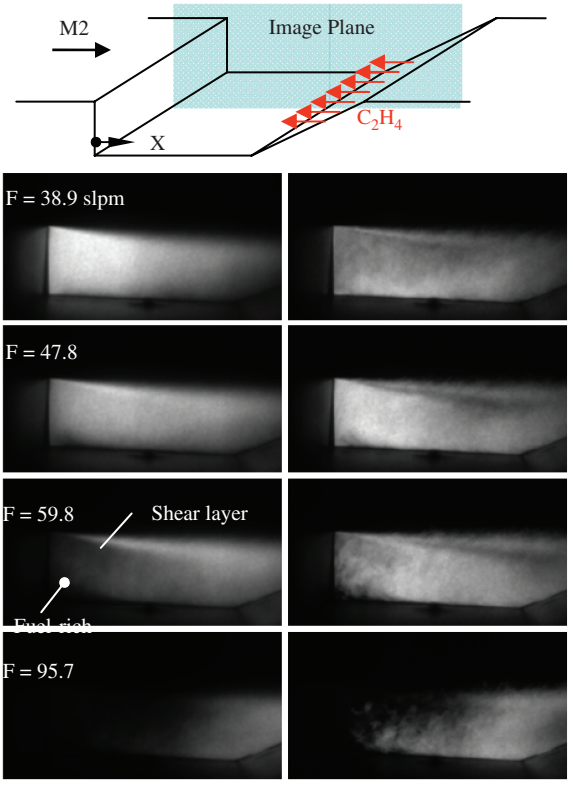

Fig. 2 EA and SD of OH along symmetrical plane with increasing cavity fuel flowrate.

rate. To allow correction of the images for perspective distortion, a *calibration* target composed of an array of dots was employed. A Matlab-based computer code that employs the *projective* algorithm was then used to correct the images. Details of the OH-PLIF technique were presented in a previous paper [1]. Shadowgraphy was also used to capture the flow features around the strut and cavity.

Probe measurements were made to obtain quantitative flow information. Probe data (Pitot and cone-static pressures and total temperature) were collected over a plane normal to the flow direction at a fixed axial location 4.45 cm downstream of the cavity. The probe was inserted through a movable probe wall and attached to a spanwise z traversing system. The probe wall was attached to the optical table, which was located below the test section to allow traversing in the y direction. By controlling the traversing system and optical table, one can collect two-dimensional (y-z plane) probe data normal to the flow direction with any desired resolution. For nonreacting flow, probe data were collected over a fixed spatial domain ($0 \le z \le 8.89$ cm and $0 \le y \le 5.08$ cm), with 0.25-cm resolution for both y and z directions. For the reacting-flow experiment, only the total-temperature probe was used to collect temperature-field data with reduced resolutions (0.51 cm× 0.51 cm) as compared with the nonreacting case. For nonreacting flow, flow quantities such as total pressure and temperature, static pressure, Mach number, and density can be reduced from raw probe data using a custom data-reduction routine.

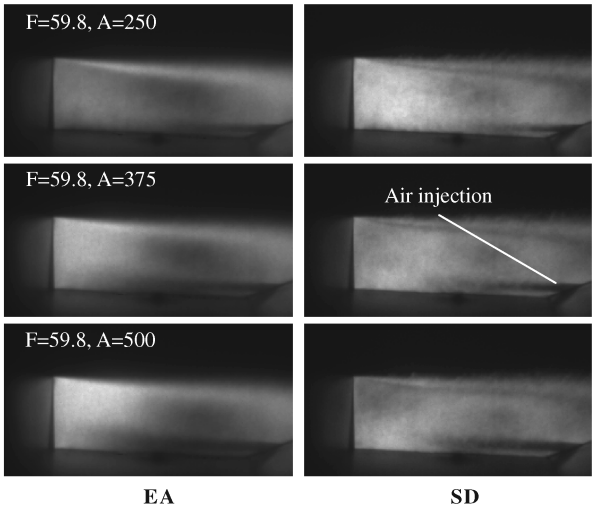

Fig. 3 EA and SD of OH distributions along symmetrical plane with various cavity air flowrates at cavity fueling of 59.8 slpm.

III. Results and Discussion

A. Baseline Cavity

For a baseline cavity flameholder with fueling from the ramp, the streamwise OH distributions along the symmetrical plane were recorded, as illustrated in Fig. 2. Ensemble-averaged (EA) and standard-deviation (SD) images were processed from multiple

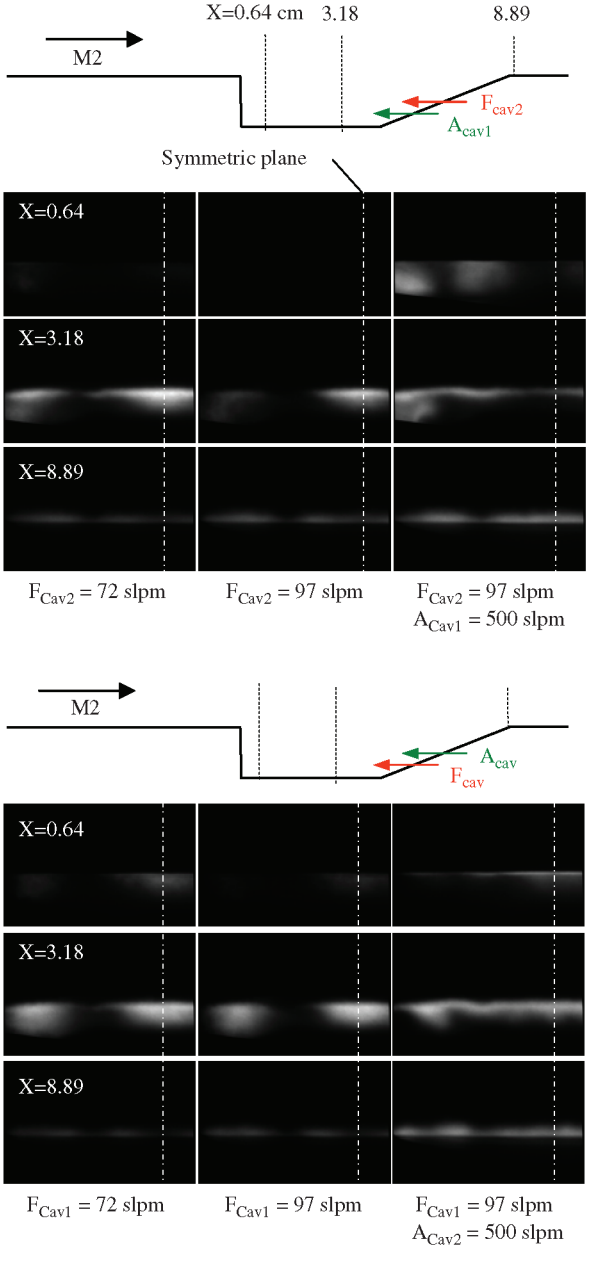

Fig. 4 End views of OH (EA) distributions for two cavity injection schemes.

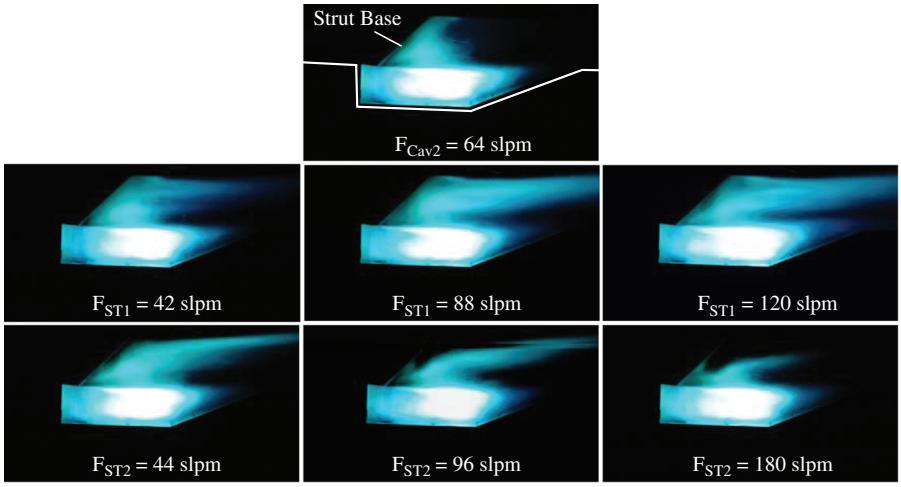

Fig. 5 Flame emission images of strut 2 with upstream F_{ST1} and downstream F_{ST2} fueling.

(typically 200) OH images for a range of cavity fuel flowrates. At low cavity fueling, the combustion filled almost the entire cavity region. Increasing the cavity fueling resulted in a fuel-rich region located near the leading edge of the cavity. With sufficient heat release, excess fuel was burned in the shear layer over the cavity. The fuel-rich region is caused by insufficient air being entrained from the main air stream to complete the combustion at higher cavity fueling. Higher fluctuations of the OH signal were observed close to the cavity floor and the leading edge of the cavity. It should be mentioned that the flowfield and combustion in the cavity are highly three dimensional and dynamic in nature [1]. To improve the cavity combustion and broaden the operation range, air was injected directly into the cavity using a row of injection ports below the fuel ports on the ramp. Figure 3 displays OH images for constant cavity fueling (59.8 slpm) and a range of cavity air flows. Clearly, the fuel-rich region at the leading edge was reduced by supplying additional direct-inject cavity air; however, a region of low OH signal was observed in the midregion of the cavity.

Two cavity fuel- and air-injection schemes (see Fig. 4) were used to assess the performance of baseline cavity combustion. One method involves injecting fuel close to the cavity floor and injecting air slightly above the fuel jets. The other method involves reversing the arrangement by injecting air closer to the cavity floor. Figure 4 shows the EA OH-PLIF images collected at different axial (x) locations using the same intensity table (spanwise view) for the two injection schemes. The cavity leading edge was used as the reference for the axial coordinate. The image covers a spatial area 8.89 cm wide by 5.08 cm high, and the left side of each image corresponds to the

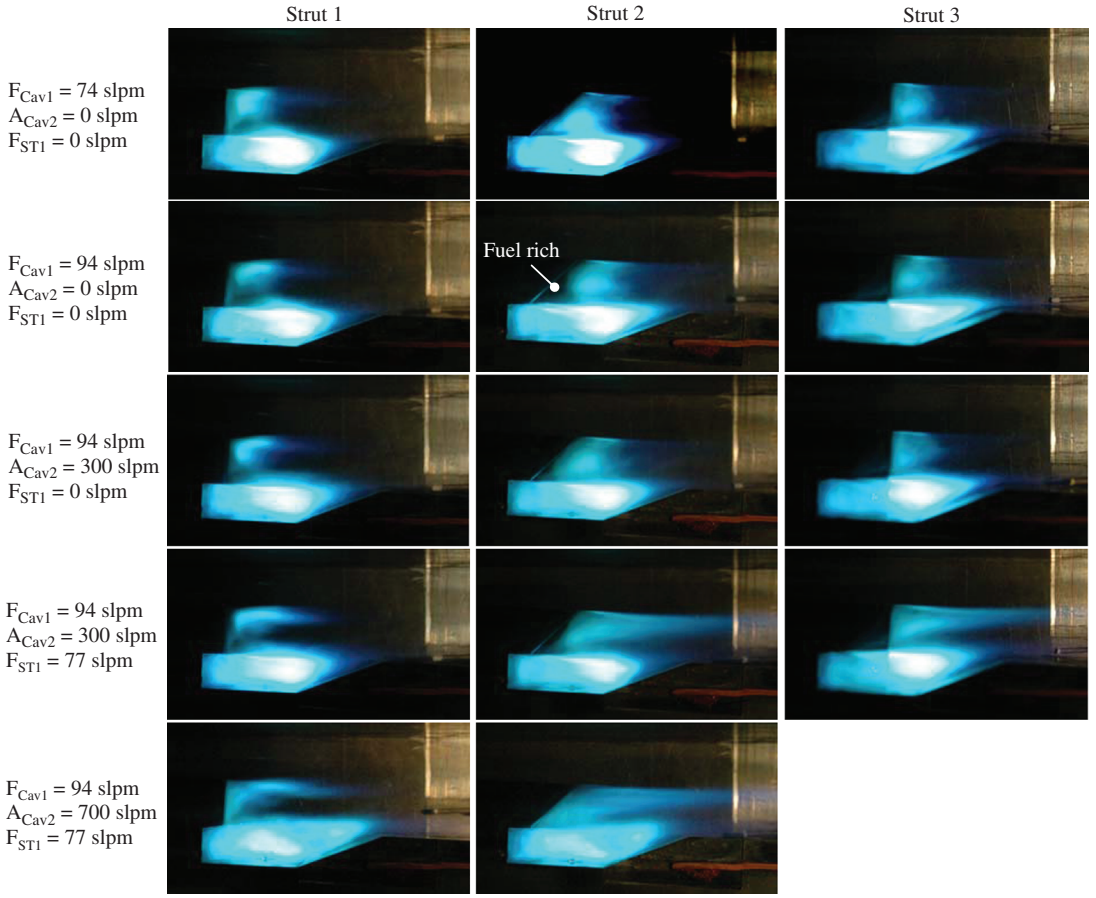

Fig. 6 Flame emission images of three different struts at various fuel and air flowrates.

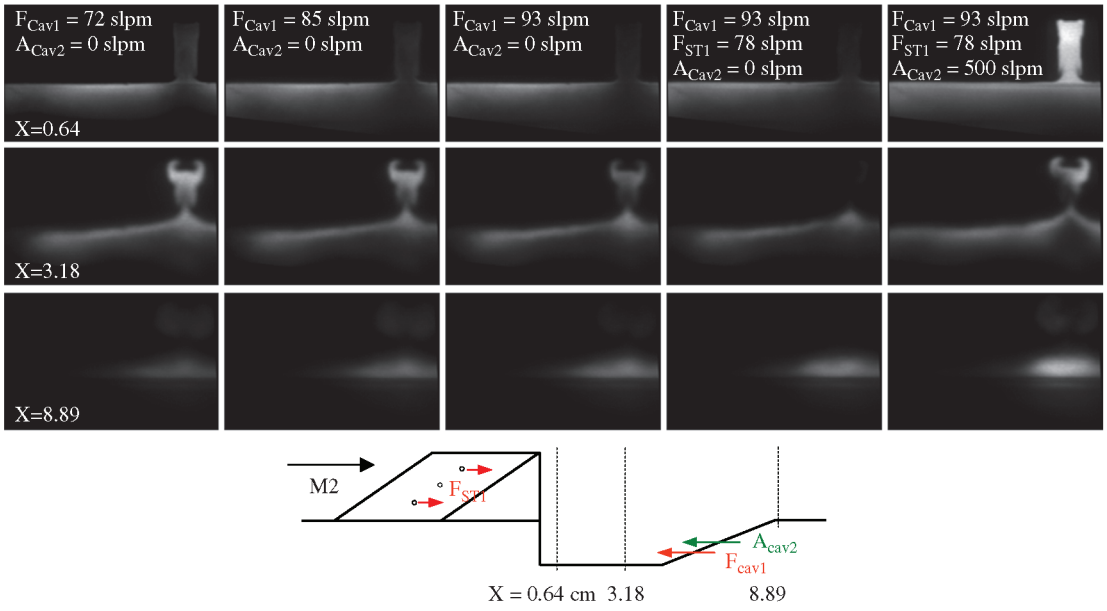

a)

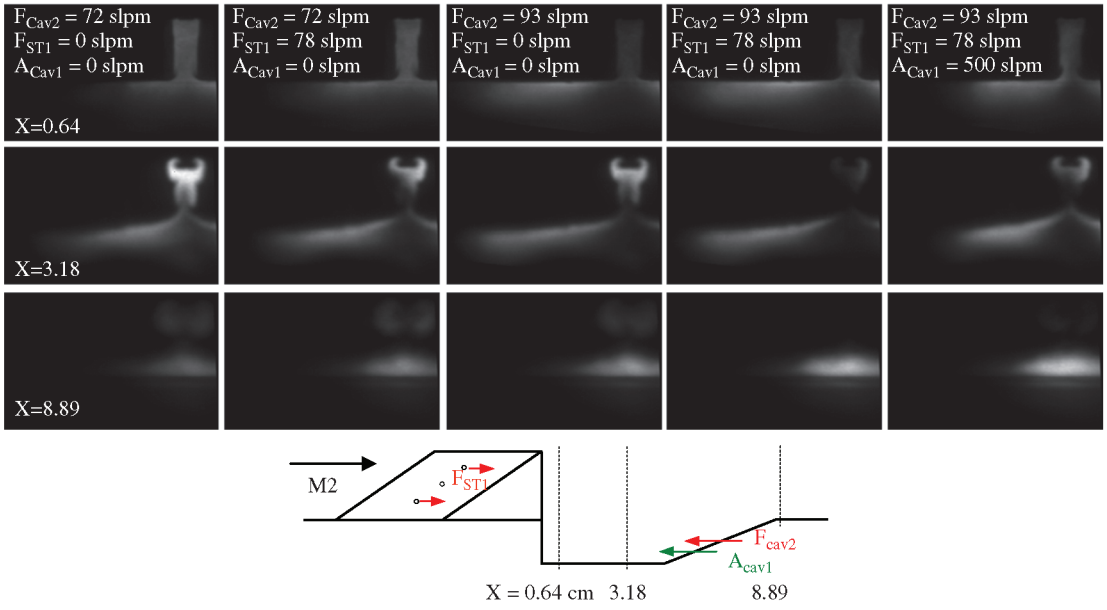

b)

Fig. 7 OH distributions using strut 1 at various cavity and strut loadings. Field of view is same as in Fig. 4.

left side-wall window. For these measurements the OH laser probe sheet was directed across the duct span while fluorescence was collected, using the PIMAX CCD camera, through the side-wall window of the tunnel (the entry window for the laser sheet). In general, a distributed combustion zone inside the cavity is evident, regardless of the injection scheme employed; and instantaneous OH images reveal the dynamic features of cavity combustion. Non-uniform combustion is evident for both fueling schemes. Fueling closer to the floor of the cavity provides a slightly broader flame zone and improves combustion in the leading edge of the cavity at higher fueling conditions. The addition of air directly into the cavity broadens the combustion zone, especially in the shear-layer region.

B. Strut Cavity

1. *Flame-Emission Imaging*

For a basic cavity flameholder, the shear layer over the top and downstream of the cavity is the region where the main fuel can be ignited effectively. For this study the interaction between the cavity and the wake created by the strut is used to enhance the region of ignition and flameholding of the main fuel. Figure 5 displays flame images recorded with strut 2 in place for two different fueling schemes at a constant cavity fueling condition. These visible chemiluminescence images were recorded using a Nikon digital camera (Model D70) integrated over the exposure of 1/640 s. Unlike the OH-PLIF data shown in Figs. 2 and 3, these flame-emission images are averages over the spanwise extent of the cavity (not just the central plane as with the OH-PLIF data). The flame behind the strut was evident with cavity fuel only. The low-pressure wake region behind the strut was found to be effective in extending the combustion out of the cavity to achieve an enlarged flameholding region. The flame propagated from the cavity fills the full strut height (2.54 cm). For upstream strut fuel injection F_{ST1}, the combustion zone behind the strut extends farther downstream with increased strut fuel and is more evident near the tip of the strut. The sweep and compression angles at the leading edge of the strut turn the flow upward, causing more strut fuel to be distributed toward the top of the strut. Combustion was found to be less intense when the downstream strut-fueling F_{ST2} scheme was used, as illustrated in Fig. 5. The downstream strut injection modifies the flow and stoichiometry in the

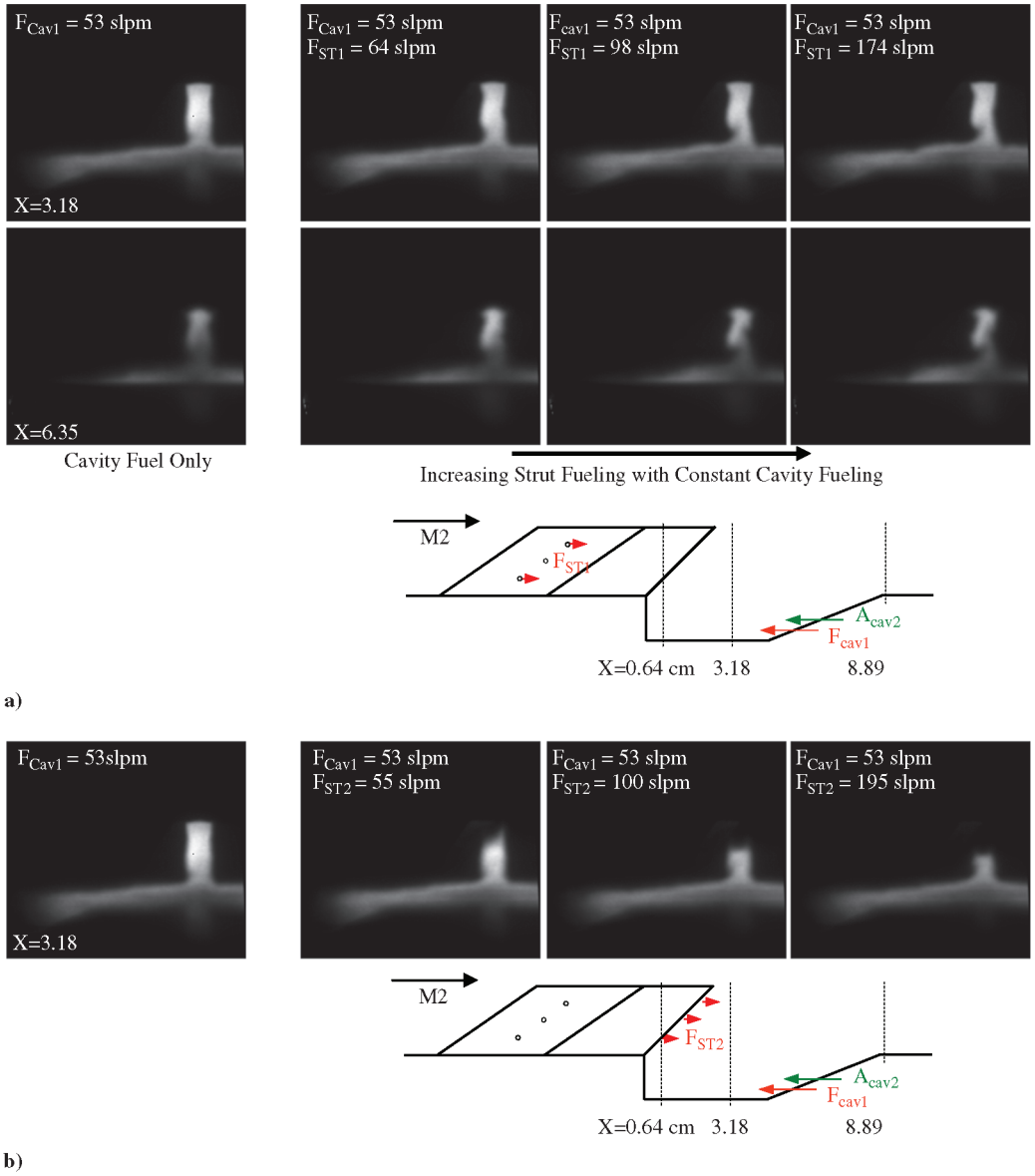

Fig. 8 Effects of strut 2 fueling schemes (upstream vs downstream) on the OH distribution. Field of view is same as in Fig. 4.

wake region where the cavity flame propagates. The area of combustion is reduced significantly with increasing downstream strut fuel. On the other hand, upstream strut fueling provides more effective mixing and sustains more combustion in the wake region.

Figure 6 displays a comparison of flame-emission images of cavity-strut combustion using three different struts operated over a range of conditions. With medium cavity fuel loading (74 slpm), the combustion zone was found to extend throughout the cavity and propagate into the wake region behind the strut. As cavity fueling increases, the flame extends farther downstream in both the cavity and the strut-wake regions. In the midheight region behind strut 2, the chemiluminescence signal is weaker, which suggests a locally fuel-rich region. When air is directly injected into the cavity, the flame appears to be more intense with reduced flame length behind the strut, which also suggests that the strut wake is mainly fuel rich. The addition of cavity air also reduces the stoichiometry behind strut 2. At moderate upstream strut fueling F_{ST1}, the increased combustion zone behind the struts is evident, especially with regard to the flame length. At the same cavity and strut-fueling condition, the strut flame appears to extend farther downstream in the strut 2 and strut 3 configurations. Combustion behind struts 1 and 2 was improved by increasing the cavity air. All three struts provide a low-pressure wake region for flame propagation and flameholding.

2. *OH-PLIF*

The PLIF technique was used to obtain spatially resolved planar distributions of the OH radical normal to the streamwise direction (as with distributions shown in Fig. 4). Figure 7 illustrates EA OH distributions with strut 1 that were collected at various cavity and strut-fueling conditions at three axial locations ($X = 0.64$, 3.18, and 8.89 cm relative to the cavity leading edge). Results of two different cavity fueling and air-injection schemes are shown in Figs. 7a and 7b. When the cavity fuel was injected closer to the cavity floor, as illustrated Fig. 7a, higher OH intensity was observed in the strut-wake region. A shear-layer flame was also evident at $X = 0.64$ cm. The OH intensity decreased with increasing cavity fuel at all three axial locations. The strut-wake region became fuel-rich as upstream strut fuel F_{ST1} was introduced. The addition of cavity air significantly improved the cavity-strut combustion, as illustrated in the figure. When the cavity fuel was injected above the cavity air, as shown in Fig. 7b, the OH intensity increased relative to that of the other cavity fueling scheme. A higher intensity of OH fluorescence was observed at a downstream location ($X = 8.89$ cm) with this cavity fueling scheme. In general, a longer residence time and more efficient mixing are achieved when fueling is closer to the cavity floor (Fig. 7a). When fuel is injected away from the cavity floor (Fig. 7b), most of the fuel is burned farther downstream, apparently because of the reduced

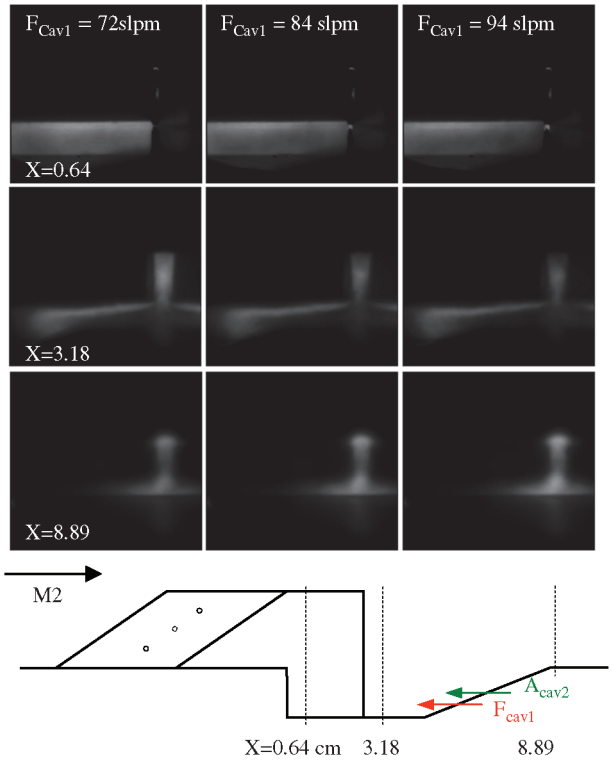

a)

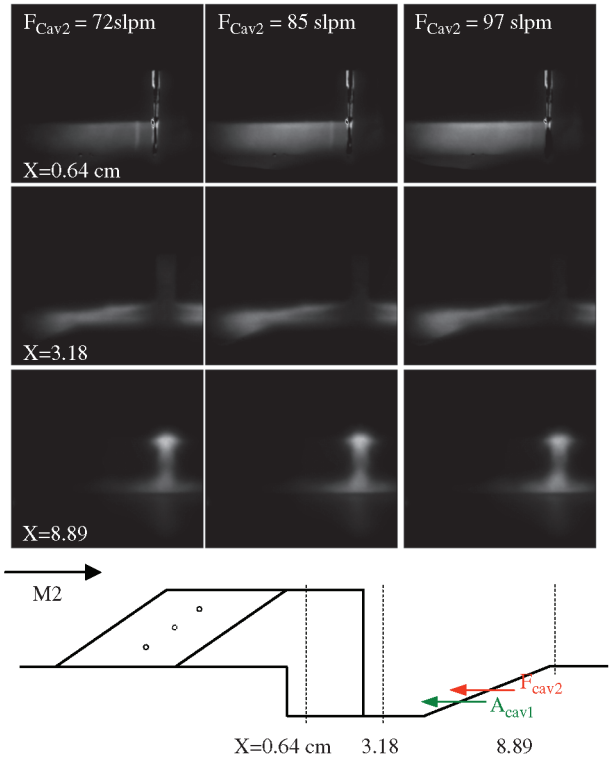

b)

Fig. 9 Effects of cavity fueling on the OH distribution with strut 3. Field of view is same as in Fig. 4.

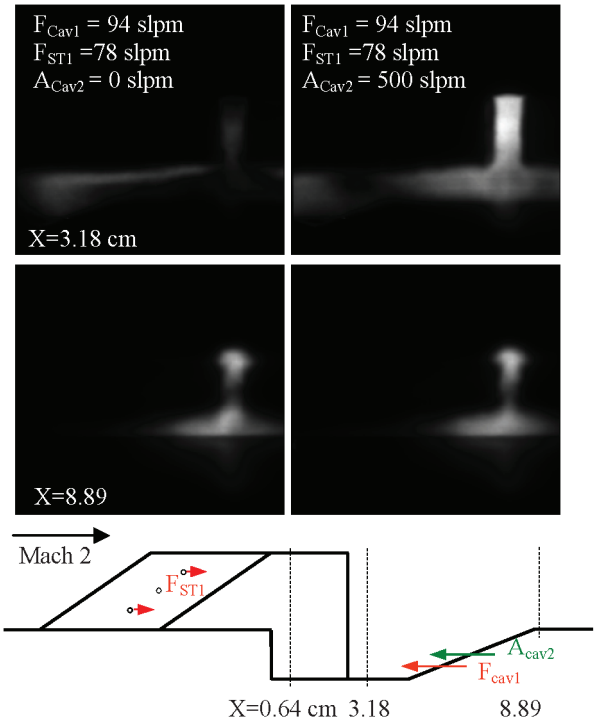

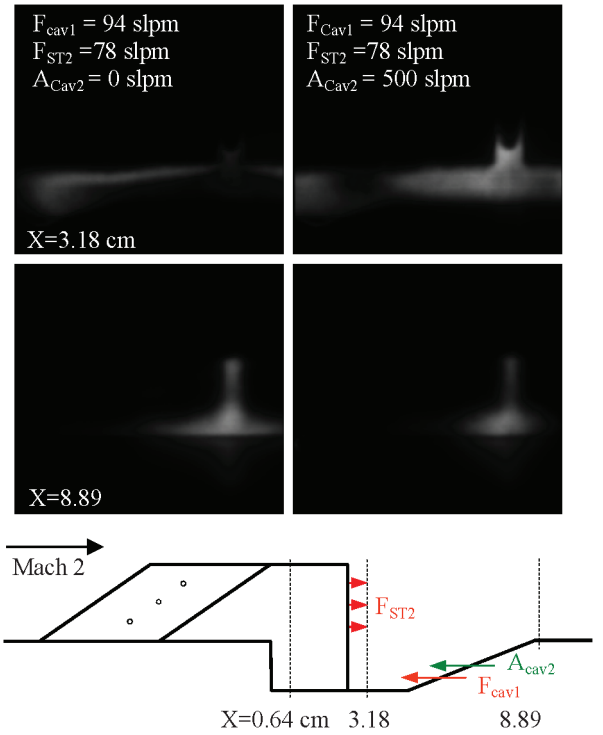

Fig. 10 Effects of strut 3 fueling schemes on the OH distribution. Field of view is same as in Fig. 4.

residence time. The distribution of OH with respect to the fueling follows the same trend for both injection schemes. Regardless of the cavity injection scheme, the OH distribution behind the base of the strut is triangular in shape and narrower at the top. This is probably due to the flow expansion toward the centerline, immediately downstream of the strut. It should be mentioned that a strong counter-rotating structure was observed at the tip of the strut wake for both injection schemes. For this strut configuration, the velocity gradient is expected to be higher near the top of the strut because of stronger flow expansion.

For strut 2 similar trends were observed for the two cavity fuel-air-injection schemes. Figure 8 shows the OH distributions for two strut-fueling schemes with the same cavity injection. Without additional cavity air, the strut wake becomes fuel rich (lower OH intensity) with increasing upstream strut fueling F_{ST1}. The asymmetry of the OH in the wake region is due to the asymmetric upstream strut injection. When the fuel was injected from the strut base F_{ST2}, the combustion in the strut wake was diminished, as shown Fig. 8b. The OH intensity

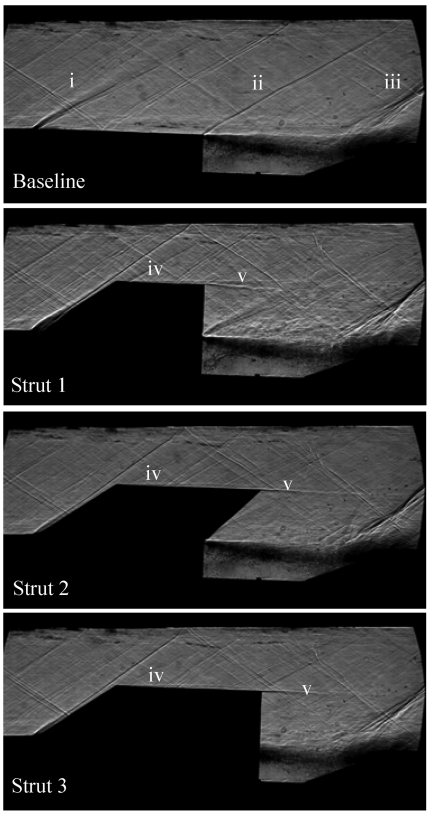

Fig. 11 Flow features illustrated by shadowgraph images.

in the wake region decreases significantly with increasing fuel flowrate for F_{ST2}. Injecting fuel from the base of the strut disrupts the low-pressure wake region that is responsible for propagating cavity combustion toward the core flow. The addition of poorly mixed fuel directly to the wake region reduces the strut combustion.

OH distributions of strut-3 combustion are shown in Figs. 9 and 10. In Fig. 9 the two different cavity injections with strut 3 installed are compared. When the cavity fuel was injected closer to the cavity floor, a fairly uniform distribution of OH was observed at $X = 0.64$ cm (see Fig. 9a). Higher OH intensity was observed in the strut-wake region ($X = 3.18$ cm), and the intensity decreased at $X = 8.89$ cm. Figure 9b shows the OH distribution when the cavity fuel was injected farther away from cavity floor. While the OH signal observed near the strut-base region ($X = 3.18$ cm) was negligible, that observed at $x = 8.89$ cm was stronger. The residence time of the cavity mixture was apparently shorter along the centerline because of the extended strut length. Combustion was delayed, with stronger combustion occurring farther downstream.

Figure 10 compares the OH distributions for two strut-fueling schemes that employ the same cavity injection method. Upstream strut injection provided better mixing and combustion in the wake region. The addition of cavity air improved the cavity and strut combustion significantly. Similar to the case of strut 2 (Fig. 8b), the strut combustion was impeded when the fuel was injected from the strut base F_{ST2}. It should be mentioned that the wake structure was similar for struts 2 and 3, with strut 1 having a very different wake structure.

3. *Shadowgraphy*

Three different struts installed upstream of the cavity introduced different flow patterns in the wake region. The main difference in these struts was the shape of the aft body. Flow features of the wake

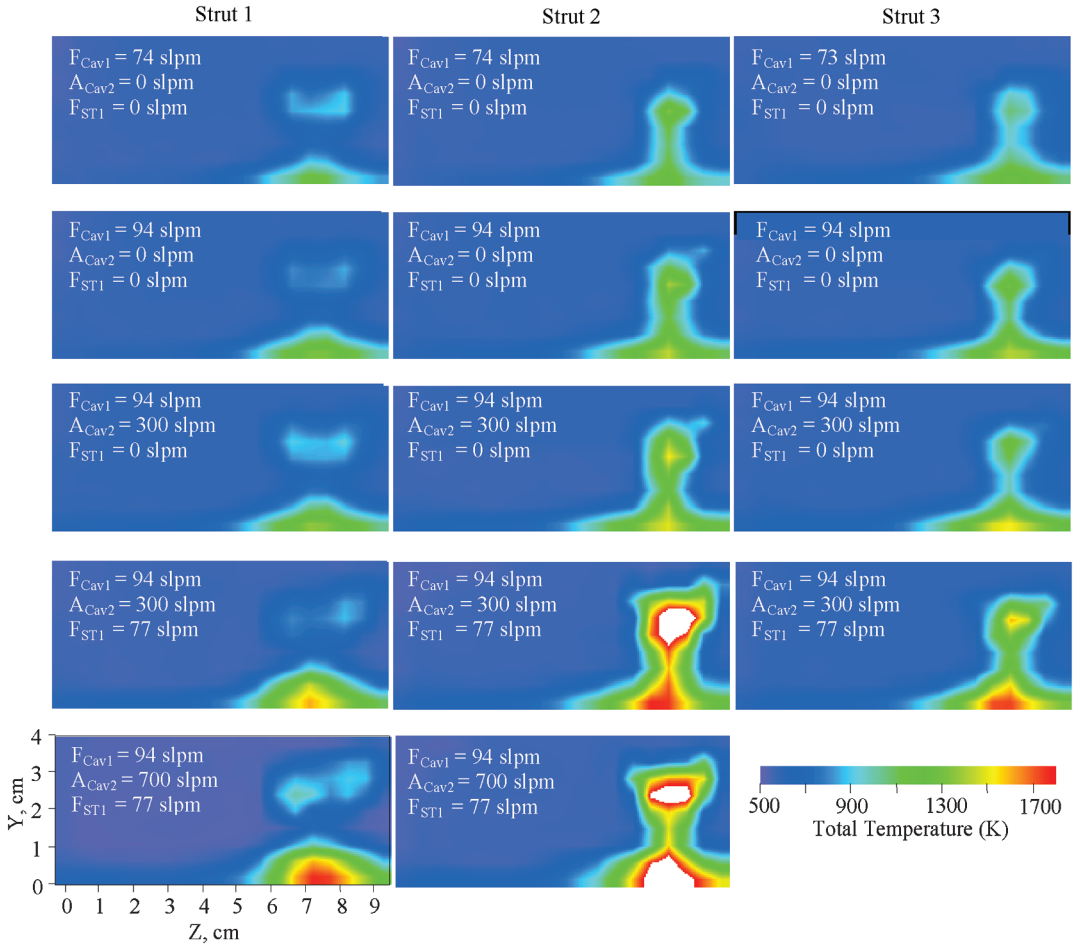

Fig. 12 Temperature distributions at various conditions measured at location $X = 4.45$ cm downstream of cavity.

region are shown in Fig. 11 with shadowgraph images. For the baseline cavity, flow expansion (labeled i in Fig. 11) was observed at the divergent location along the bottom wall, 7.62 cm upstream of the cavity. Another weak expansion wave (labeled ii) was located at the cavity leading edge. The shear layer can be clearly identified along the bottom wall and over the cavity. A series of recompression waves (labeled iii) emanating from the cavity ramp was observed. A distinct compression wave (labeled iv) could be observed just upstream of each strut. The flow was compressed along the leading edge of the strut and was diverted from the bottom wall. This flow diversion is thought to be the mechanism for transporting upstream-injected strut fuel toward the tip of the strut, especially for strut 1. Vortex shedding (labeled v) generated near the tip of the strut was also observed for all three struts, and this structure is largest for strut 1. A pair of counter-rotating streamwise vortices is responsible for the OH structure that was observed near the tip of the strut 1 (see Fig. 7). Strut 1 is the shortest (in length) of the three, and the flow expansion at the base of strut 1 should be much greater than that of the others. The velocity gradient along the perimeter of the base of strut 1 should also be greater because the flow expansion is faster than that of struts 2 and 3 (see Fig. 1). The larger shear layer generated at the top of strut 1, as shown in Figs. 7 and 11, is a result of the unique flow structure behind this strut.

4. *Probe Data*

A total-temperature probe was used to collect temperature profiles for all three struts operating over a range of reacting flow conditions. Figure 12 shows temperature contours for all three struts to permit a direct comparison. Although strut 1 produces a wider flame zone in the wake of the strut than struts 2 and 3, the peak temperature is lower than that of struts 2 and 3 operated at similar conditions. Combustion downstream of the cavity was concentrated near the centerline as a result of the influence of the strut. The combustion zones of the strut-wake and cavity regions appear to be disconnected in strut 1, which is consistent with the chemiluminescence and OH-PLIF images shown in Figs. 6 and 7. Similar temperature contours were observed for struts 2 and 3 operated at similar conditions, except that strut 2 exhibited much higher temperature in the core of the strut wake and cavity centerline at higher fuel and air flows. Strut 2 also has a larger wake-combustion region than strut 3. A triangle-shape region appears to connect the cavity and strut wake along the centerline for all three struts. This region results from flow expansion toward the centerline near the base of the aft body.

Probe measurements were conducted in the nonreacting flow as well, also at $X = 4.45$ cm. Figure 13 shows contours of reduced Mach number, total pressure, and stream thrust for all three struts. The strut-wake region has both low total pressure and low Mach number, providing a region for flame propagation from the cavity and sustained combustion for upstream strut fueling. The main difference in the Mach contours of the struts involves the shape of the wake. Strut 1 has the largest low-Mach wake region. The shape of the total-pressure contour is similar to that of the Mach contour for the corresponding strut configuration. Strut 3 has the lowest total pressure in the strut-wake region because of its length (which creates more flow losses). The wake shapes correlate well with the total-temperature contours obtained from reacting cases (see Fig. 12). The flow structure created by the strut and its interaction with the cavity flow is a deciding factor in how efficiently the fuel is mixed and burned. Stream thrust is calculated by $m \bullet V + P \bullet A$ at each probing location, where m is the mass flux, V the axial velocity, P the static pressure, and A the area defined by the probe sampling density (0.25 cm $\times$ 0.25 cm). Strut 1 has a slightly higher stream thrust distribution than the other two struts. Spatially integrated stream thrust over the probe domain is also slightly higher for Strut 1, but among the struts the difference is negligible.

IV. Conclusions

Cavity combustion in a Mach 2 crossflow was studied using 1) planar laser-induced fluorescence of the OH radical, 2) chemiluminescence imaging, 3) shadowgraphy, and 4) probe sampling to quantify total temperature and pressure, Mach number, and stream thrust. The cavity was designed to have fuel or air inject directly from the ramp face through three rows of fueling ports (located at different heights along the ramp face) for varying the fuel-air equivalence ratio within the cavity. Slight differences in flame distribution were observed for the two cavity fueling schemes; injecting the cavity fuel closer to the floor provides more efficient combustion as a result of improved mixing and residence time. The addition of air directly into the cavity broadens the combustion zone, especially in the shear-layer region.

A strut injector was installed on the symmetric plane upstream of the cavity to provide an alternative method for improving ignition and flame propagation and for sustaining combustion in the core flow of a supersonic combustor. Three different strut injectors differing primarily in their aft body were evaluated; and in all three cases, fuel injected upstream along the strut face burned more effectively.

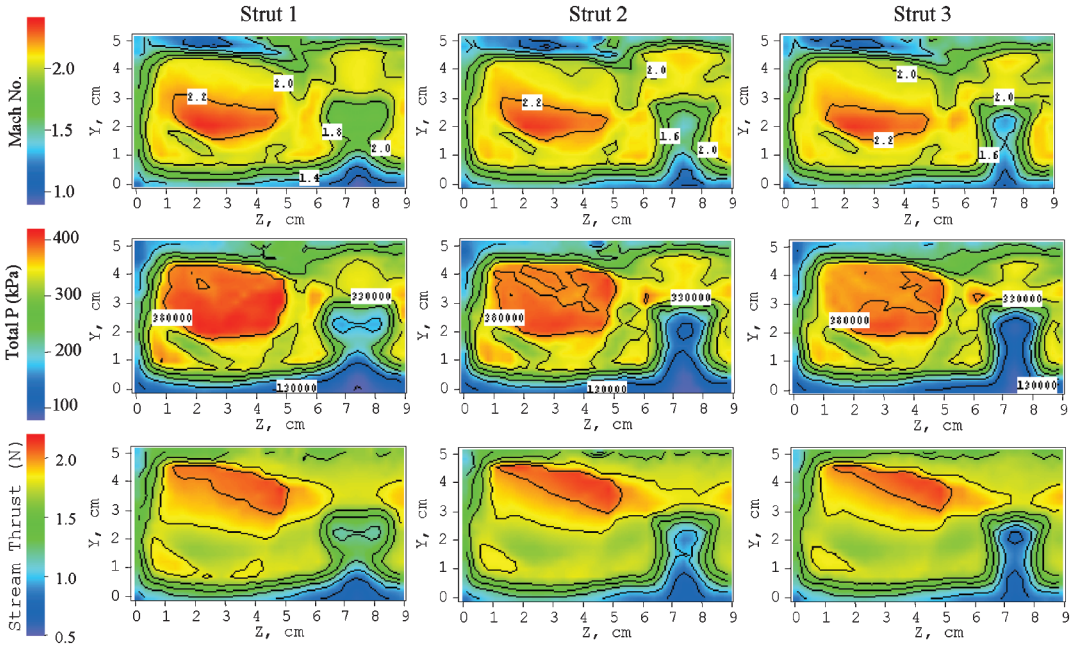

Fig. 13 Contours of Mach number, total pressure, and stream thrust for three struts in nonreacting flow ($P_0 = 345 \pm 4$ kPa and $T_0 = 294 \pm 1.5$ K).

Different strut-wake shapes were observed as a result of the modification of the flowfield around the strut and cavity regions. The addition of fuel directly in the wake of the strut created a fuel-rich zone that inhibited the effective burning of the strut fuel and disrupted the wake flow. Direct cavity air injection improved combustion in the cavity (as in the case without the strut) and strut-wake regions dramatically, which could potentially broaden the operation range of the cavity flameholder.

Finally, from the sampling probe measurements, higher total temperatures in the reacting flows were observed for strut 2 than for the other two at higher fuel and cavity air flows. In addition, strut 1 appears to have a slightly larger wake than the other two. However, the difference in the integrated stream thrust was negligible among the three struts.

Acknowledgments

This work was sponsored by the U.S. Air Force Office of Scientific Research and the U.S. Air Force Research Laboratory Propulsion Directorate under Contract F33615-03-D-2327. The authors would like to thank Robert Behdadnia for his support. The assistance of G. Streby, D. Schommer, and W. Terry and of B. Brantley in preparing and conducting experiments is also appreciated. The support of the Research Air Facility of the U.S. Air Force Research Laboratory Propulsion Directorate is acknowledged.

References

[1] Gruber, M. R., Donbar, J. M., Carter, C. D., and Hsu K.-Y., "Mixing and Combustion Studies Using Cavity-Based Flameholders in a Supersonic Flow," *Journal of Propulsion and Power*, Vol. 20, No. 5, 2004, pp. 769–778.
doi:10.2514/1.5360

[2] Rasmussen, C. C., Driscoll, J. F., Carter, C. D., and Hsu, K. -Y., "Characteristics of Cavity-Stabilized Flame in a Supersonic Flow," *Journal of Propulsion and Power*, Vol. 21, No. 4, 2005, pp. 765–768.
doi:10.2514/1.15095

[3] Allen, W., King, P. I., Carter, C. D., Gruber, M. R., and Hsu, K.-Y., "Fuel-Air Injection Effects on Combustion in Cavity-Based Flameholders in a Supersonic Flow," AIAA Paper 2005-4105, 10–13 July 2005.

[4] Edens, S., King, P. I., Gruber, M. R., and Hsu, K.-Y., "Performance Measurements of Direct Air Injection in a Cavity-Based Flameholder for a Supersonic Combustor," AIAA Paper 2006-4861, 9–12 July 2006.

[5] Bogdanoff, D., "Advanced Injection and Mixing Techniques for Scramjet Combustors," *Journal of Propulsion and Power*, Vol. 10, No. 2, 1994, pp. 183–190.
doi:10.2514/3.23728

[6] Sunami, T., Marge, P., Bresson, A., Grisch, F., Orin, M., and Kodera, M., "Experimental Study of Strut Injectors in a Supersonic Flow Using OH-PLIF," AIAA Paper 2005-3304, 16–20 May 2005.

[7] Tomioka, S., Murakami, A., Kudo, K., and Mitani, T., "Combustion Tests of a Staged Supersonic Combustor with Strut," *Journal of Propulsion and Power*, Vol. 17, No. 2, 2001, pp. 293–300.
doi:10.2514/2.5741

[8] Desikan, S., and Job, K., "Mixing Studies in Supersonic Flow Employing Strut Based Hypermixers," AIAA Paper 2005-3643, 10–13 July 2005.

[9] Lahr, M. D., Pitz, R. W., Douglas, Z. W., and Carter, C. D., "Hydroxyl-Tagging Velocimetry Measurements of a Supersonic Flow over a Cavity," *Journal of Propulsion and Power*, Vol. 26, No. 4, July–Aug. 2010, pp. 790–797.

[10] Grady, N. R., Pitz, R. W., Carter, C. D., Friedlander, T., and Hsu, K.-Y., "Hydroxyl Tagging Velocimetry in a Supersonic Flow over a Piloted Cavity," AIAA Paper 2010-1405, Jan. 2010.

[11] Smith, S., Scheid, A., Eklund, D., Gruber, M., Wilkin, H., and Mathur, T., "Supersonic Combustion Research Laboratory Uncertainty Analysis," AIAA Paper 2008-5065, July 2008.

C. Segal
Associate Editor